**COMET WILD 2 DUST: HOW PARTICLE STRUCTURE AND COMPOSITION ARE REFLECTED IN THE SHAPE OF STARDUST AEROGEL TRACKS.**

M. C. Price[1] , A. T. Kearsley[2], M. J. Burchell[1], R. Abel[2] and M. J. Cole[1]. [1] mcp2@star.kent.ac.uk, School of Physical Science, University of Kent, Canterbury, CT2 7NH, UK., [2] IARC, Department of Mineralogy, The Natural History Museum, London, SW7 5BD, UK

**Introduction:** Silica aerogel has proven to be an effective capture medium for deployment in space missions [1]. On the Stardust spacecraft it successfully collected a large number of dust particles from comet 81P/Wild 2 [2-4]. Earlier orbital aerogel collectors [e.g. 5] and laboratory light gas gun (LGG) experiments [6] showed that impacting grains leave distinctive penetration tracks, whose size depends on impactor mass and velocity. Stardust track shape has been classified into three types [4]: Type A, an elongate and narrow stylus, which may divide; Type B, with a bulbous proximal portion with one or more styli in the distal region; Type C, broad and bulbous with no elongate styli.

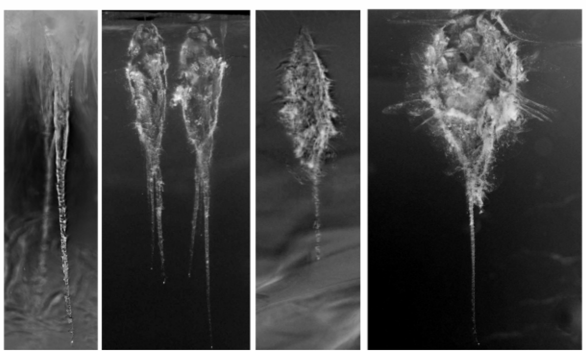

Figure 1. Stardust aerogel track morphology showing the transition (left to right) from: Type A (left) through B, almost to C. Images courtesy of NASA/Stardust Preliminary Examination team.

Type A tracks have been created in LGG shots of many robust projectiles [e.g. 4,7], but Type B and C have only been reproduced in a few unusual cases, e.g. porous grains of the microcrystalline hydrous serpentine mineral Lizardite make small Type B tracks [4]. Theoretical models [8] suggest that mechanical break-up of aggregate impactors is the main mechanism responsible for Type C (and probably Type B) tracks, with expansion of volatile components playing little part. In this paper we describe the results of new LGG experiments at 6.1 km $s^{-1}$ (appropriate for simulation of the Stardust Wild 2 encounter), using artificial mineral aggregates that survive LGG acceleration [9] and generate a wide range of track shapes. Using a suite of organic projectiles, we also explore the importance of volatile expansion in creation of bulbous Type C tracks.

**Experimental hypervelocity impact program:** Track shapes were compared for 5 types of projectile fired as sabot-filling powders at ~ 6 $kms^{-1}$ in the LGG at Canterbury, using the protocol of [10]:

*Mineral powders:* A wide range of anhydrous silicate and sulfide minerals, produced by pestle and mortar crushing of subsamples selected from the collection of the Natural History Museum (NHM), as in [11];

*Basalt glass:* A powder prepared from a crushed and sieved sample of USGS NKT-1G, as used in [12];

*Lizardite serpentine:* a porous, natural aggregate material of fine hydrated silicates [4], powdered.

*Fine-grained artificial mineral aggregates*: prepared by the method of [9], using acrylate spray adhesive. Size separation of subgrains was performed by timed aqueous column sedimentation for silicates < 4 µm, and magnetic separation through micropore filters for pyrrhotite fractions of < 10 µm and < 20 µm.

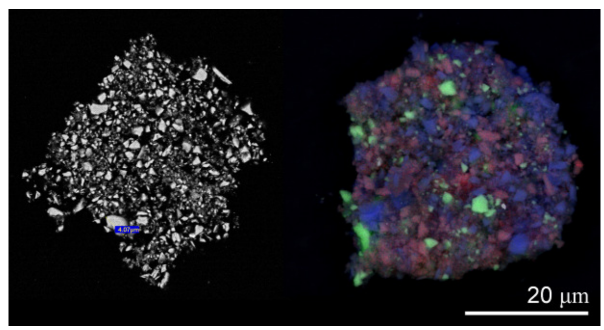


Figure 2. Aggregate projectiles used in this study. Left: BEI of a polished section through a monodisperse olivine aggregate; Right: superimposed BEI (grey) and EDX maps for Mg (blue), Ca (red) and Fe (green) showing the rough surface of a polymineralic olivine, diopside and pyrrhotite aggregate.

*Organic materials:* Glycine (powder from Sigma Aldrich), Urea (crystallized from a dissolved mixture of $^{15}$N-labelled and normal urea) , PMMA (Poly (methylmethacrylate)) spheres, and POM (Poly (oxymethylene)) polydisperse powder, filed from a polymer block supplied by Goodfellow.

Impacted aerogel targets were photographed with back lighting, and image contrast was inverted for clarity of detail. Selected examples were imaged by scanning electron microscopy with energy dispersive X-ray (EDX) microanalysis, and by X-ray micro Computed Tomography (CT) imaging at NHM.

**Results from laboratory experiments:**

*Robust anhydrous mineral and basalt impacts*

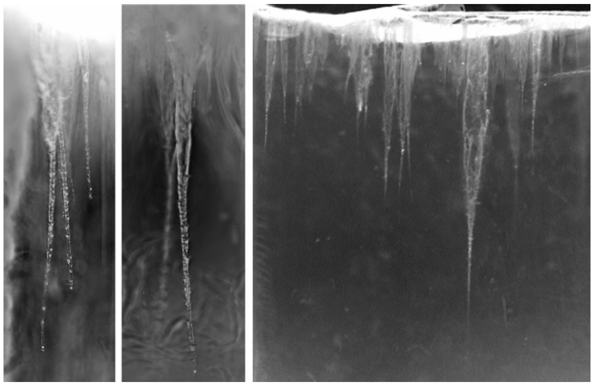

Figure 3. Type A tracks, optical images of impacts by (left to right) basalt glass, enstatite and pyrrhotite.

*Natural hydrous silicate mineral aggregates*

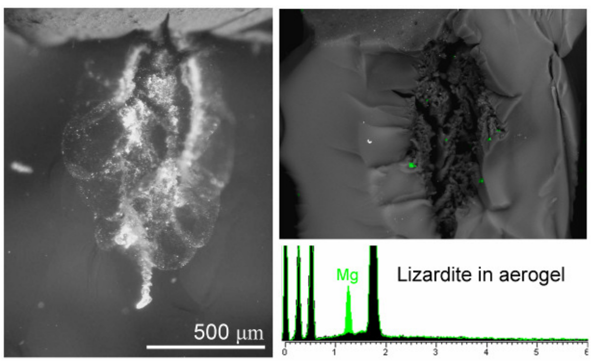


Figure 4. Type B track, with preserved mineral fragments (green). Optical (left) and backscattered electron (right) images of impact by lizardite serpentine. Note short stylus with terminal grain in left image.

*Artificial mineral aggregates and organics*

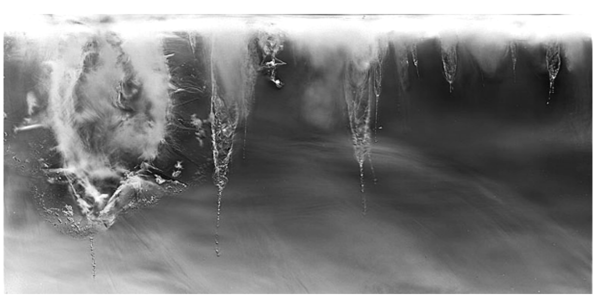

Figure 5. Type B and C tracks, optical image of block impacted by artificial aggregates containing fine monodisperse fine diopside and coarser pyrrhotite. Proportion of Type B increases with pyrrhotite size.

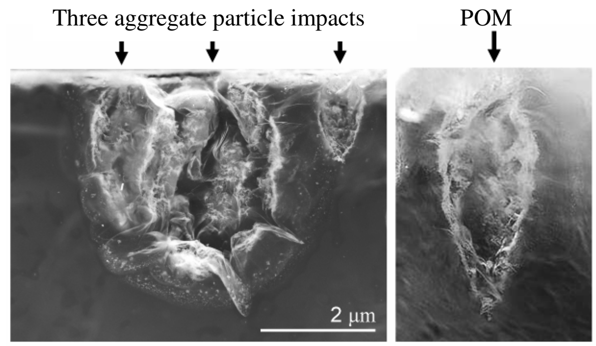


Figure 6. Type C tracks, optical images of: (left) three impacts by artificial polymineralic aggregates made of a mixture of monodisperse olivine, diopside and pyrrhotite, bound by acrylate adhesive; and (right) an impact by an organic POM powder grain.

**Discussion:** Our results show that Type B tracks can be made by impact of aggregate particles containing coarser mineral subgrains bound by organic matter in a finer mineral matrix. Type C tracks can be produced by impact of organic-bound aggregates of monodisperse fine mineral powders, or even by some pure organic materials such as POM (postulated to be present in cometary dust [13]), glycine and urea, although other delicate organic materials (such as PMMA and PST) create tracks of Type A shape, similar to glass, silicate and sulfide mineral grains.

**Conclusions:** LGG experiments have now reproduced the range of aerogel track morphology seen in the Stardust collection of Wild 2 comet dust. Internal grain-size range within aggregates and the presence of labile organic matter exert a strong control on aerogel track shape. Experimental evidence shows that diverse subgrain size within aggregate particles encourages Type B track formation, and that volatile expansion probably plays a greater role in the creation of Type C aerogel tracks than previously suggested [8].

**References:** [1] Burchell M.J. et al. (2006) *Ann. Rev. Earth Plan. Sci.* 34, 385-418. [2] Brownlee D.E. et al. (2006) *Science, 314,* 1711-1716. [3] Hörz F. et al. (2006) *Science, 314,* 1716-1719. [4] Burchell M.J., et al. (2008) *MAPS,* 43, 23 – 40. [5] Hörz F. et al.. (2000) *Icarus* 147, 559–79 [6] Hörz F. et al. (1998) NASA TM-98-201792, 58 pp. [7] Burchell M.J. et al. (2001) *MAPS,* 36, 209–21 [8] Trigo-Rodríguez J.M. et al. (2008) *MAPS,* 43, 75–86. [9] Kearsley A.T. et al. (2009) *MAPS,* 44, 1489-1509. [10] Burchell M.J. et al. (1999) *Meas. Sci. Tech.,* 10, 41–50 [11] Kearsley A.T. et al. (2008) *IJIE,* 35, 1616-1624. [12] Marcus M.A. et al. (2008) *MAPS,* 43, 87–96. [13] Cottin H. et al (2004) *Icarus* 167, 397–416.